Facile hydrothermal synthesis of economically viable VO2(M1) counter electrode for dye sensitized solar cells

Facile hydrothermal synthesis of economically viable VO_2(M1) counter electrode for dye sensitized solar cells

Geeta R. Mutta[1*], Srinivasa R. Popuri[2], M. Vasundhara[3], Michal Maciejczyk[4], Andrei V. Racu[5], Radu Banica[5], Neil Robertson[4], John I. B. Wilson[6], Nick S. Bennett[1]

[1]Nano-Materials Laboratory, School of Engineering and Physical Sciences, Heriot-Watt University, Edinburgh EH14 4AS, United Kingdom

[2]Institute of Chemical Sciences, School of Engineering and Physical Sciences, Heriot-Watt University, Edinburgh EH14 4AS, United Kingdom

[3]Materials Science and Technology Division, CSIR-National Institute for Interdisciplinary Science and Technology, Industrial Estate, Trivandrum 695019, India

[4]School of Chemistry and EaStCHEM, University of Edinburgh, Edinburgh EH9 3FJ, United Kingdom

[5]National Institute for Research and Development in Electrochemistry and Condensed Matter, Dr. A. Paunescu Podeanu str. 144, Timisoara, Romania

[6]Institute of Photonics and Quantum Sciences, School of Engineering and Physical Sciences, Heriot-Watt University, Edinburgh EH14 4AS, United Kingdom

*Corresponding author: geeta.mutta@gmail.com

Abstract

In this study, we focus at reducing the fabrication cost of dye sensitized solar cells (DSSCs). Sphere-like VO_2(M1) polymorph was synthesized by single step facile hydrothermal approach using citric acid as the reducing agent. Phase purity, charge state and surface morphology of the synthesized product was confirmed by X-ray diffraction, X-ray photoelectron spectroscopy and scanning electron microscopy respectively. The electrochemical impedance and cyclic voltammograms of VO_2 films indicated a good electrocatalytic activity towards redox reaction of the I^-/I_3^- shuttle. Owing to the low cost, low-temperature processing and good catalytic activity, in this work we propose to use VO_2 as a counter electrode to substitute the expensive platinum

electrode in DSSCs. By means of VO_2 based DSSCs we achieved a **five**fold reduction in the cost to energy conversion efficiency ratio. It is expected that with further optimization, VO_2 can be exploited as a good candidate for counter electrode in DSSC technology.

Keywords: A. layered compounds; B. oxides; C. chemical synthesis; D. impedance spectroscopy; E. catalytic properties

1. Introduction

Draining of natural resources is bringing a global energy crisis, ever closer yet solutions are possible such as a shift to renewable energy sources. Solar energy is the largest natural energy resource which can be explored and utilized much more generously [1]. Dye sensitized solar cells (DSSCs) technology which convert light into electricity has gained a lot of attention due to their key features such as low fabrication cost, environmental compatibility, price-to-performance ratio, ability to work at wider angles and in low light [2,3]. A typical DSSC consists of a metal oxide as an active electrode, a light harvesting dye, a redox electrolyte and a counter electrode (CE). The chief concern in the commercialization of DSSCs is cutting down the manufacturing cost further, while keeping up decent efficiencies and lifetime. The principle production cost of DSSCs depends on the materials cost and fabrication process. The CE is a vital component which transfers the electrons from the external circuit to the internal electrolyte and as a whole, reduces the tri-iodide ions to iodine ions, which eventually realizes the operation of DSSCs.

Conventionally, platinum (Pt) on fluorine doped tin oxide (FTO) coated glass is used as a CE. Platinum is chosen because of its high electrocatalytic activity, conductivity and chemical affinity to reduce tri-iodide [4]. However, the major concern here is, Pt being expensive and having limited natural availability which primarily restricts the production of DSSCs at large

scale. Hence, there is a pressing need for the identification of economically viable CE materials, exhibiting high photovoltaic performance and stability. Thus many researchers have been focusing on alternative materials to Pt with similar characteristics. In the recent years, the number of reports concerning the alternative CEs has increased significantly. For the current state of art of Pt-free CEs, the reader may refer to review papers elsewhere [4-9]. Apart from high catalytic activity and high electrical conductivity, the prime characteristics for choosing an alternative material for CEs are abundance in nature, environmentally friendly, stability and economic viability for large scale production.

Transitional metal oxides (TMOs) are of particular interest for this type of application, because of their excellent atmospheric stability, low cost, abundance in nature, good catalytic and electrical conductivities. Despite these advantages less effort has been devoted to exploit TMOs as CEs until this decade. Recently TMOs such as WO_2, WO_3, ZrO_2, TiO_2, Cr_2O_3, MoO_2, Nb_2O_5, NiO, V_2O_5 and V_2O_3 are reported as CEs in electrolyte based DSSCs and V_2O_5 composite in solid state DSSCs [10-15]. In TMOs family, vanadium based oxides are receiving huge interest in the field of energy storage technologies such as batteries and super capacitors, because of their diverse chemical motifs, layered structure, high energy capacity and moderate work functions [16,17]. From the economical point of view, the raw materials cost of vanadium based oxides estimated from Sigma-Aldrich catalogue show 30 times less than that of Pt of the same purity level. The VO_2 compound exhibits several stable polymorphs such as VO_2(M1), VO_2(R), VO_2(B), VO_2(A), VO_2(D), VO_2(BCC) and VO_2(N) [18]. In particular the VO_2(M1) polymorph has attracted tremendous attention for electronic, thermochromic and optical applications such as smart windows and electrical switches [19-21]. In this work, we propose and demonstrate VO_2(M1) to be used as a CE in DSSCs.

To the best of our knowledge, it is the first time that VO_2(M1) has been explored as a CE in DSSC technology. We report here a simple hydrothermal route to synthesize the pure VO_2(M1) polymorph. We have carried out detailed characterization of synthesized product and investigated the photovoltaic performance for VO_2(M1) CEs in DSSCs.

2. Experimental

2.1. Materials synthesis

The synthesis of VO_2(M1) via a hydrothermal process is as follows: Initially V_2O_5 (Aldrich) was dissolved in 35 mL of deionized water. After stirring for 15 min using a magnetic stirrer, 1.5 molar ratio to V_2O_5 of citric acid monohydrate ($C_6H_8O_7 \cdot H_2O$; Merck) was added into the solution and stirring was prolonged for another 15 min. The resultant yellowish green aqueous solution was transferred into the Teflon lined stainless steel autoclave. The sealed steel autoclave was placed in a high temperature oven at 250 °C. After 24 hrs, the autoclave was slowly cooled to room temperature naturally. The as obtained bluish-black powder samples were filtered and washed several times with distilled water and ethanol to remove unreacted chemical species and dried in air at 80 °C for 6 hrs and then used for further characterizations.

2.2. Fabrication of dye sensitized photoelectrodes

The photoelectrodes (PEs) are prepared as follows: first FTO coated glass substrates (Pilkington TEC glass™, sheet resistance: 11.7 Ω/sq, 2.2 mm in thickness, TEC-12) were cut into small pieces (2 × 2 cm). The substrates were first cleaned thoroughly with Teknon microcleanse detergent solution, ultrasonicated in deionised water followed by acetone and iso-propanol for 15 min at each step, and then dried in flowing nitrogen to further remove any solvent traces. Afterwards the substrates were transferred into a 40 mM $TiCl_4$ solution container

and heated for 1 hour at 80 °C to form a compact layer of TiO_2. Later the substrates were rinsed thoroughly with deionised water followed by dry in flowing nitrogen. Commercial nanocrystalline TiO_2 paste (DSL 18NR-T, Dyesol as the transparent layer) was screen printed on the compact layered FTO substrates, afterward TiO_2 scattered paste (DSL 18NRAO, Dyesol as the scattering layer) was deposited by screen printing. The active screen printed areas were approximately 1 cm^2. The TiO_2 coated films were then successively sintered in ambient on a hotplate in a series of steps such as at 325 °C for 10 min, at 375 °C for 5 min, at 450 °C for 15 min and at 500 °C for 15 min, and finally were cooled down naturally to room temperature. Later these electrodes were further treated with 40 mM $TiCl_4$ for 30 min at 80 °C and consequently sintered at 450 °C for 30 min and then allowed for cooling. As soon as these photoelectrodes reach 80 °C, these films were subsequently immersed in N719 (Dye-sol) solution and kept in an air-tight glass container at room temperature under dark and dry conditions for 20 hours. Dye sensitized photoanodes were rinsed with iso-propanol followed by drying with nitrogen flow at room temperature.

2.3. Fabrication of counter electrodes

First a small hole was drilled on FTO coated glass substrates using a sand blasting unit, with a smooth finish given by ending the drilling with a portable glass hole drilling tool. These drilled FTO substrates were subjected to the same cleaning and drying processes as aforementioned. A thick viscous paste of VO_2 was prepared by mixing 4:1 ratio of hydrothermally synthesized VO_2 powder and ethyl cellulose and by adding few drops of α-terpineol. This paste was deposited on FTO coated glass by screen printing and later sintered at 450 ºC for 30 mins under inert atmosphere at a heating rate of 5 ºC/min to remove the organic

binders. Reference electrodes were prepared by depositing Pt on FTO glass substrates by means of sputtering.

2.4. Photovoltaic cell assembly

The N719 dye sensitized TiO_2 PEs and CEs were assembled into a sandwich configuration with a spacer between the two electrodes. Subsequently the liquid electrolyte (composed of 0.05 M Iodine, 0.1 M lithium iodine, 0.6 M 1-butyl-3-methylimidazolium iodide and 0.5 M 4-tertbutyl pyridine in a mixture of acetonitrile and valeronitrile) was injected via drilled hole into the space between these electrodes. Finally the holes were sealed with a polymer film of 25 μm thickness (Metlonix 1170, Dupont surlyn) and glass cover. The schematic of the final assembled device is shown in Fig. 1.

2.5. Material and device characterizations

The phase purity and crystallographic structure of VO_2 powder was determined using automated PANalytical X' Pert Diffractometer, Netherlands (using Ni filtered Cu $K_{\alpha 1}$ radiation, λ=1.5406 Å). To further access information about the degree of oxidation of vanadium and thereby the composition and the electronic structure of VO_2, we carried out X-ray photoelectron spectroscopy (XPS) measurements on powder sample at room temperature. The XPS spectrum was acquired using a Kratos Analytical AMICUS XPS instrument and a Mg $K_{\alpha 1}$ X-ray source operated at 150 W (10 kV, 15 mA). The surface morphology of VO_2 powder sample and the screen printed VO_2 CE was investigated by field emission scanning electron microscopy (FESEM) (XL30 ESEM). The photocurrent density and photovoltage characteristics of DSSCs were measured by computer controlled digital source meter (Keithley 2400) under AM 1.5 one sun (100 $mWcm^{-2}$) illumination using a solar simulator (92250 A, Newport, USA). An

electrochemical work station system (Autolab potentiostat equipped with FRA2 module) was employed to measure the internal resistances of the assembled final cells. Cyclic voltammetry measurements over the VO_2 and Pt CEs were performed at room temperature using a μAUTOLAB Type III Potentiostat set-up which was driven by the electrochemical software GPES.

3. Results and discussion

3.1. Structural and morphological characterization

In order to know the phase formation and the crystallinity of the as synthesized powder samples, X-ray diffraction (XRD) study was carried out at room temperature. Fig. 2a shows the XRD patterns of the as-prepared VO_2 powder and as well as VO_2 CE. For the same XRD acquisition time, the stronger diffraction peaks observed in the case of CE indicates that thermal annealing improved the crystallinity. All the diffraction peaks exhibited in the XRD patterns can be readily assigned to the monoclinic phase of VO_2(M1) (JCPDS card no. 01-082-0661). The room temperature crystal structure details are determined from Le bail fits using the FullProf program [22]. In the case of powder and thin film samples, the lattice parameters are extracted as a=5.753(3) Å, b=4.532(3) Å, c=5.364(1) Å, β=122.40(2)º and a=5.7503(4) Å, b=4.5246(3) Å, c=5.3812(4) Å, β=122.59(2)º respectively. No diffraction peaks corresponding to any other vanadium oxide phases are detected either in the powder sample or from the screen printed CE.

To further access information about the degree of oxidation of vanadium and thereby the composition and the electronic structure of VO_2, we carried out XPS measurements on powder sample at room temperature. The XPS spectrum shown in Fig. 2b revealed binding energy levels that correspond to vanadium and oxygen (which are the chemical elements in VO_2) and atmospheric carbon. No other peaks of impurity elements are noticed. For our XPS analysis, the

binding energy (BE) of the adventitious carbon C 1s = 284.6 eV is taken as an energy calibration reference. Fig. 2b inset shows the valence band (VB) region and core level spectra for vanadium and oxygen elements in VO_2. The high resolution XPS VB region consists of V 3d and O 2p levels in the energy ranges between 0-2 and 3-9 eV, respectively as shown in the inset of Fig. 2b. The zero spectral weight at the Fermi level supports the nonmetallic behavior of VO_2(M1) at room temperature. From core level XPS spectra, we noticed the BE levels of V $2p_{3/2}$ and O 1s peaks which are centered at 516.41 eV and 529.84 eV, respectively (see Fig. 2b). These are characteristic energy levels of the V^{4+} oxidation state and in good agreement with most of the reported values. Besides the V^{4+} $2p_{3/2}$ core level one more minor contribution is visible around 517.15 eV. From the literature, it is clear that this BE level corresponds to V^{5+} $2p_{3/2}$ and this could be due to surface oxidation of the VO_2 powder samples [23]. Similarly a second component is visible in the O 1s signal at 531.2 eV. It can be attributed to surface contamination by atmospheric carbon. The O 1s BE reported for C=O is within 530.7–531 eV and the extra shoulder to the O1s peak (531.2 eV) thus falls into the region of C=O O 1s. In addition, this is also consistent with the components in the C 1s spectrum where we found a shoulder at 287.6 eV, which is a 3.0 eV higher binding energy than the C–C bond (284.6 eV) [24]. Due to a wide spread in the XPS BE values reported for vanadium oxides, Mendialdua *et al.* proposed that difference in binding energies between the O 1s core level and the V $2p_{3/2}$ core level (ΔE= BE(O1s)–BE(V $2p_{3/2}$)) is a better determination of vanadium oxidation degree [25]. According to this, ΔE is between 17.65-17.90 eV, 16.33-18.4 eV, 14.2-14.85 eV, 13.45-14.5 eV and 12.6-12.9 eV for V^0, V^{2+}, V^{3+}, V^{4+} and V^{5+} oxidization degrees, respectively. In our case, the BE difference (ΔE) between the vanadium core level (V $2p_{3/2}$) and the oxygen core level (O 2p) is 13.65 eV.

This is in agreement with +4 oxidation degree of V and confirms the chemical composition as VO_2.

For further studying the structure feature, the morphology and microstructure of VO_2 powder and the screen printed VO_2 CE was observed using FESEM. Fig. 3 displays the SEM images of both powder and thin film CE. The low magnification image as seen in Fig. 3a, clearly depicts evidence of large-scale uniformity of the hydrothermally synthesized VO_2. The zoom view of the marked area in this image shows the specimen is mainly composed of a mass of spheres and a small 'fluffy' structure. Further close inspection reveals these spherical structures to resemble that of woolen balls with diameters ranging from hundreds of nanometers to about 7 micron. The morphology of an annealed VO_2 film is shown in Fig. 3c and Fig. 3d, which appears to be dense and uniform without cracks. Fig. 3d shows the high magnification image of the marked area in Fig. 3c. In comparison to the original appearance of as synthesized powder, the screen printed film has an obvious change in the morphology, which is reflected by the presence of fewer spherical structures, as some of these micro spheres are crushed into smaller particles during the grinding process while making the viscous paste for screen printing.

3.2. Photovoltaic performance

Fig. 4 displays the photocurrent density - photovoltage (J-V) curves of the device characteristics of DSSCs with VO_2 and sputtered Pt CEs. These results were obtained using the sandwich structure shown in Fig. 1. The photovoltaic parameters of these devices including series and shunt resistances (R_s and R_{sh}) are summarized in the Table 1. The DSSC with VO_2 CE yielded an overall photoconversion cell efficiency (η) of 1.25%, short-circuit photocurrent density (J_{sc}) = 4.67 $mAcm^{-2}$, open-circuit photovoltage (V_{oc}) = 0.61 V, fill factor (FF) = 43.72%. The results of DSSCs with conventional Pt electrodes produced of 7.08% (J_{sc}=14.90 $mAcm^{-2}$,

V_{oc} = 0.64 V, FF = 73.74%). The V_{oc} of both the samples are similar, as the photoanode and the dye are the same, whereas the lower values of J_{sc} and FF in VO_2 CE indicating towards less utilization efficiency of photogenerated electrons than that of Pt CE [26]. R_s and R_{sh} values are extracted from the inverse slopes of the light J-V curves. Both cells exhibit a similar R_{sh} of about 2.8 $K\Omega cm^{-2}$, whereas R_s values of 27 and 5 Ωcm^{-2} for VO_2 and Pt were respectively. The inferior efficiency of VO_2 based cells to that of Pt based DSSCs is mainly linked to low FF. It is known that the FF is influenced by R_s and R_{sh} of the solar cell. The FF reflects the extent of electrical and electrochemical losses during DSSC operation. As both cells exhibit similar R_{sh} value, it implies that further understanding of R_s is crucial. This will help to decrease R_s value to eventually increase the corresponding FF. To ensure reproducibility of the DSSCs, six cells of VO_2 DSSCs were fabricated and tested.

3.3. Electrochemical characterization

In order to better understand the electrocatalytic performance of proposed CE towards the reduction of I_3^-, electrochemical impedance spectroscopy (EIS) measurements were conducted on full cells fabricated with CEs of VO_2 and for reference Pt CEs was used. The impedance spectra were collected under dark conditions at a bias of 0.8 V in the frequency range 0.1 Hz to 1 MHz. The obtained Nyquist plots of Pt and VO_2 full cells are displayed in Fig. 5a and Fig. 5b, respectively. The EIS spectra exhibited two semicircles, which describe the different impedance contributions of DSSC. In case of Pt the semicircles are well defined whereas in VO_2 (M1), the semicircles are convoluted. In inset figure the encircled portion of Fig. 5b data is plotted in close up for better visibility. The first semicircle in the high frequency region (on the extreme left) describes the charge transfer resistance at the CE/electrolyte interface (R_{ct}). The R_{ct} is determined by the diameter of the high frequency semi-circle in the Nyquist plots and its

magnitude is our main focus since the CE used for DSSCs is responsible for this. It is known that the total internal series resistance of a DSSC is the sum of sheet resistance of the transparent conducting oxide substrates, R_{ct} and the diffusion resistance of I_3^- ions in the electrolyte. In this work, all the devices are assembled using the same photoanode and electrolyte except the counter electrode. This suggests the different internal series resistance values obtained can be attributed to the Ohmic losses in the electrolyte and between the electrolyte and the counter electrode layer. From Nyquist plots, it is evident that the magnitude of R_{ct} of a VO_2 based DSSC is relatively higher than that of conventional Pt based one. This indicates that the total internal impedance of the VO_2 DSSC is higher which has a direct influence on the electron transport mechanism in DSSCs. As an effect, the cell performance of the VO_2 based DSSCs is lower compared to conventional Pt, which is in consonance with J-V curves.

To further evaluate the catalytic activity of the proposed CE towards the iodine/tri-iodide (I^-/I_3^-) redox couple is studied by cyclic voltammetry (CV). The CV spectra were recorded at a scan rate of 50 mV/s in a three electrode system in a freshly prepared anhydrous acetonitrile solution containing 0.1 M $LiClO_4$, 10 mM LiI and 1 mM I_2, which was purged with nitrogen prior to each measurement. The three electrode system comprised of Ag/AgCl as the reference electrode, Pt wire as the counter electrode and sputtered Pt or VO_2 screen printed on FTO glass as the working electrode. Cyclic voltammograms of I^-/I_3^- redox mediator on both Pt and VO_2 CEs are shown in Fig. 6. The Pt CE shows two pairs of distinctive redox peaks at E_{ox1}= 524 mV, E_{red1}= 91 mV and E_{ox2}= 997 mV, E_{red2}= 665 mV which demonstrates its good catalytic activity.

The lower potential redox pair is attributed to the oxidation and reduction of I^-/I_3^- whereas the higher potential pair is assigned to the oxidation and reduction of I_2/I_3^-. The VO_2 CE has shown one broad oxidation peak at lower potential E_{ox1}= 161 mV and a reduction peak whose

value is not well defined. Peak to peak separation (EPP) is an important parameter, which qualifies the catalytic activity of CEs. The EPP value for the Pt electrode was found to be 524 mV but due to the broad reduction of VO_2 CE the EPP value could not be estimated. The increase in interfacial charge transfer resistance in the VO_2 based DSSC obtained from EIS spectra lowers the FF of the device, which is the main reason for low photovoltaic efficiency and is further supported by its corresponding CV performance. Furthermore, enhancement of electrical conductivity of VO_2 can be achieved by tuning the electronic properties by means of doping with elements such as Mo and W. Along with doping, the other possibility to promote the electrical conductivity is by preparing VO_2/carbon composites. The number of reaction sites for catalytic activity can be upgraded by tuning the morphology of the synthesized product. It is believed combining both of the aforementioned steps certainly will enhance the utilization efficiency as a result of enhancement of the charge transfer ability and the number of reaction sites [27].

4. Conclusion

In summary, our report shines light on the potential of an inexpensive, abundant and easily scalable material as a CE in DSSC technology to replace the popular choice Pt which prohibits the large scale production because of its cost. The VO_2(M1) polymorph has been investigated as an alternative CE material in DSSCs. We have synthesized VO_2 using a single step, simple hydrothermal synthesis. The phase confirmation of the synthesized product was done by XRD and XPS. The SEM micrographs evidence that the VO_2 powder is composed of uniformly distributed spherical particulates. The CV and EIS studies demonstrate the electrocatalytic activity of the screen printed VO_2 CEs. The photoconversion efficiency of the best cell achieved was 1.25%. These results revealed that the V_{oc} and R_s of the DSSC obtained

using VO_2 as the CE are significant in the first attempt of study though inferior to that of the DSSCs made of Pt CEs. Our future investigations will be focused on enhancing the efficiency, the stability and the long term operation of DSSCs made with VO_2 CEs. Though the obtained efficiencies are still below that of Pt, these primary results are encouraging and provide a scope to the search for abundant and low cost, environmentally friendly materials as an effective alternate for DSSCs.

Acknowledgements

Dr. J. Buckman of Institute of Petroleum Engineering, Heriot-Watt University (HWU) is gratefully acknowledged for the access to SEM facilities and G.R.M thanks A. Boccolini of HWU for some scientific discussions. Part of this work was supported by the Council of Scientific and Industrial Research, Govt. Of India, sponsored projects (CSC0132 and CSC0122), Board of Research in Nuclear Sciences and EPSRC Supersolar Hub.

References

[1] M. A. Hasan, and K. Sumathy, Renewable and Sustainable Energy Reviews **14** (7), 1845 (2010).

[2] B. O'regan, and M. Grätzel, Nature **353** (6346), 737 (1991).

[3] M. Grätzel, Prog. Photovoltaics: Res. Appl. **14** (5), 429 (2006).

[4] M. Wu, and T. Ma, ChemSusChem **5** (8), 1343 (2012).

[5] M. Wu, and T. Ma, J. Phys. Chem. C **118** (30), 16727 (2014).

[6] S. Yun, A. Hagfeldt, and T. Ma, Adv. Mater. **26** (36), 6210 (2014).

[7] M. Ye, X. Wen, M. Wang, J. Iocozzia, N. Zhang, C. Lin, and Z. Lin, Materials Today **18** (3), 155 (2015).

[8] S. Yun, Y. Liu, T. Zhang, and S. Ahmad, Nanoscale **7** (28), 11877 (2015).

[9] J. Theerthagiri, A. R. Senthil, J. Madhavan, and T. Maiyalagan, ChemElectroChem **2** (7), 928 (2015).

[10] M. Wu, X. Lin, Y. Wang, L. Wang, W. Guo, D. Qi, X. Peng, A. Hagfeldt, M. Grätzel, and T. Ma, J. Am. Chem. Soc. **134** (7), 3419 (2012).

[11] M. Wu, X. Lin, A. Hagfeldt, and T. Ma, Chem. Commun. **47** (15), 4535 (2011).

[12] J. WeiáGuo, and H. GuiáYang, Chem. Commun. **49** (53), 5945 (2013).

[13] J. Xia, C. Yuan, and S. Yanagida, ACS Appl. Mater. Interfaces **2** (7), 2136 (2010).

[14] D. Paul Joseph, M. Saravanan, B. Muthuraaman, P. Renugambal, S. Sambasivam, S. Philip Raja, P. Muthuraaman, and C. Venkateswaran, Nanotechnology **19**, 485707 (2008).

[15] G. R. Mutta, S. R. Popuri, M. Maciejczyk, N. Robertson, M. Vasundhara, J. Wilson and N. Bennett, Materials Research Express **3**, 035501 (2016).

[16] W. Cheng, G. Zeng, and M. Niederberger, J. Mater. Chem. A **3** (6), 2861 (2015).

[17] M. Yu, Y. Zeng, Y. Han, X. Cheng, W. Zhao, C. Liang, Y. Tong, H. Tang, and X. Lu, Adv.

Funct. Mater. **25**, 3534 (2015).

[18] S. R. Popuri, A. Artemenko, C. Labrugere, M. Miclau, A. Villesuzanne, and M. Pollet, J. Solid State Chem. **213**, 79 (2014).

[19] S. R. Popuri, M. Miclau, A. Artemenko, C. Labrugere, A. Villesuzanne, and M. Pollet, Inorganic Chemistry **52** (9), 4780 (2013).

[20] J. Zhou, Y. Gao, Z. Zhang, H. Luo, C. Cao, Z. Chen, L. Dai, and X. Liu, Scientific Reports **3**, 3029 (2013).

[21] P. Markov, R. E. Marvel, H. J. Conley, K. J. Miller, R. F. Haglund Jr, and S. M. Weiss, ACS Photonics **2** (8), 1175 (2015).

[22] J. Rodríguez-Carvajal, Physica B: Condensed Matter **192** (1), 55 (1993).

[23] N. Alov, D. Kutsko, I. Spirovova, and Z. Bastl, Surface Science **600** (8), 1628 (2006).

[24] G. Silversmit, D. Depla, H. Poelman, G. B. Marin, and R. De Gryse, J. Electron Spectroscopy and Related Phenomena **135** (2), 167 (2004).

[25] J. Mendialdua, R. Casanova, and Y. Barbaux, J. Electron Spectroscopy and Related Phenomena **71** (3), 249 (1995).

[26] Z. L. Ku, X. Li, G. H. Liu, H. Wang, Y. G. Rong, M. Xu, L. F. Liu, H. Hu, Y. Yang, H. W. Han, J. Mater. Chem. A **1**, 237 (2013).

[27] M. Shahpari, A. Behjat, M. Khajaminian, and N. Torabi, Solar Energy **119**, 45 (2015).

Table 1. Photovoltaic parameters of DSSCs using VO_2 and Pt CEs.

Counter Electrode	**V_{oc} (V)**	**J_{sc} ($mAcm^{-2}$)**	**FF (%)**	**η (%)**	**R_s (Ωcm^{-2})**	**R_{sh} ($K\Omega cm^{-2}$)**
VO_2	0.61	4.67	43.72	1.25	27	2.84
Pt	0.64	14.90	73.74	7.08	5	2.85

Figure captions page

Fig. 1. Schematic representation of the assembled liquid based DSSC. It is comprised of transparent conducting oxide (FTO) on glass, a nanoparticle photoelectrode (such as TiO_2) sensitized with N719 dye, hole-conducting iodine based liquid electrolyte and platinum or VO_2 deposited on FTO coated glass back contact.

Fig. 2. Powder XRD patterns of VO_2 powder and screen printed VO_2 CE; star symbol represents the Bragg reflections from the FTO coated glass substrate; bottom green markers highlight the Bragg reflection positions associated with VO_2(M1) (JCPDS card number 01-82-0661) (b) Core level XPS spectra of V $2p_{3/2}$ and O 1s. Inset shows the high resolution valence band region of VO_2(M1) XPS spectra.

Fig. 3. SEM images of VO_2 powder: (a) at low magnification, (b) at higher magnification; screen printed VO_2 thin films: (c) at low magnification, (d) at higher magnification.

Fig. 4. The J-V curves of the DSSCs fabricated with VO_2 and Pt counter electrodes, respectively.

Fig. 5. Nyquist plots of full cells assembled with VO_2 and Pt counter electrodes, respectively.

Fig. 6. Cyclic voltammograms of VO_2 and Pt counter electrodes measured at a fixed scan rate of 50 mVs^{-1} using three electrode configurations.

Fig. 1

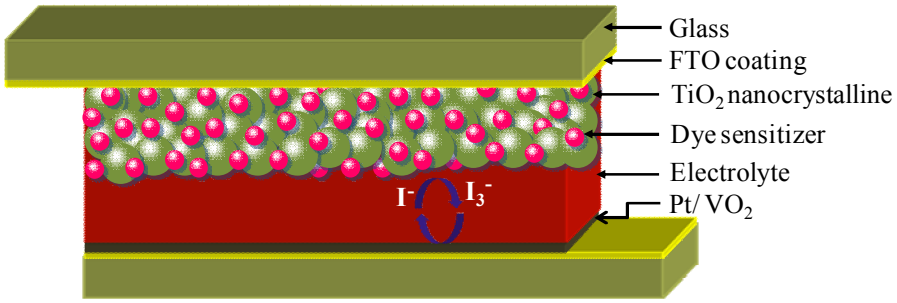
Glass
FTO coating
TiO_2 nanocrystalline
Dye sensitizer
Electrolyte
Pt/ VO_2
I^-
I_3^-

Fig. 2

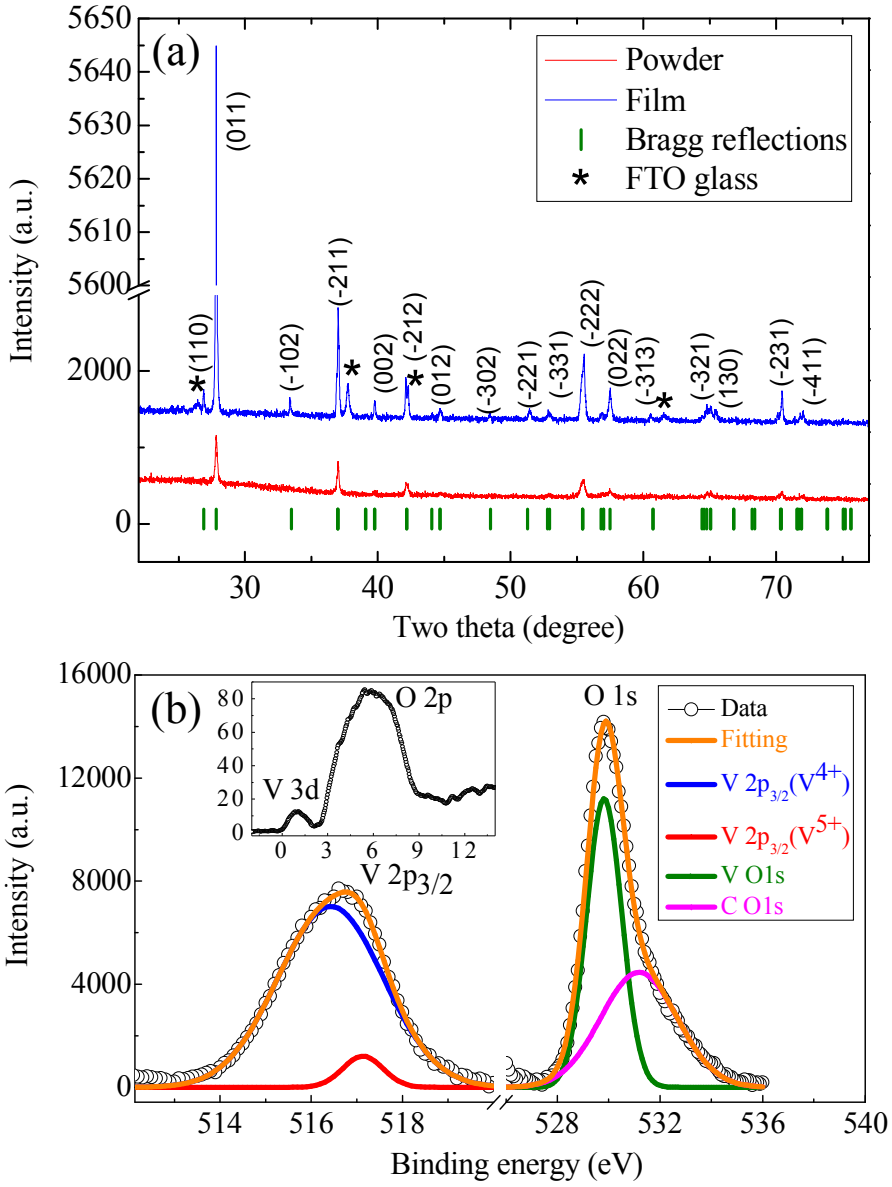
(a)
Powder
Film
Bragg reflections
FTO glass
(011)
(110)
(-102)
(-211)
(002)
(-212)
(012)
(-302)
(-221)
(-331)
(-222)
(022)
(-313)
(-321)
(130)
(-231)
(-411)
Intensity (a.u.)
Two theta (degree)
(b)
O 2p
V 3d
V 2p3/2
O 1s
Data
Fitting
V 2p3/2(V4+)
V 2p3/2(V5+)
V O1s
C O1s
Intensity (a.u.)
Binding energy (eV)

Fig. 3

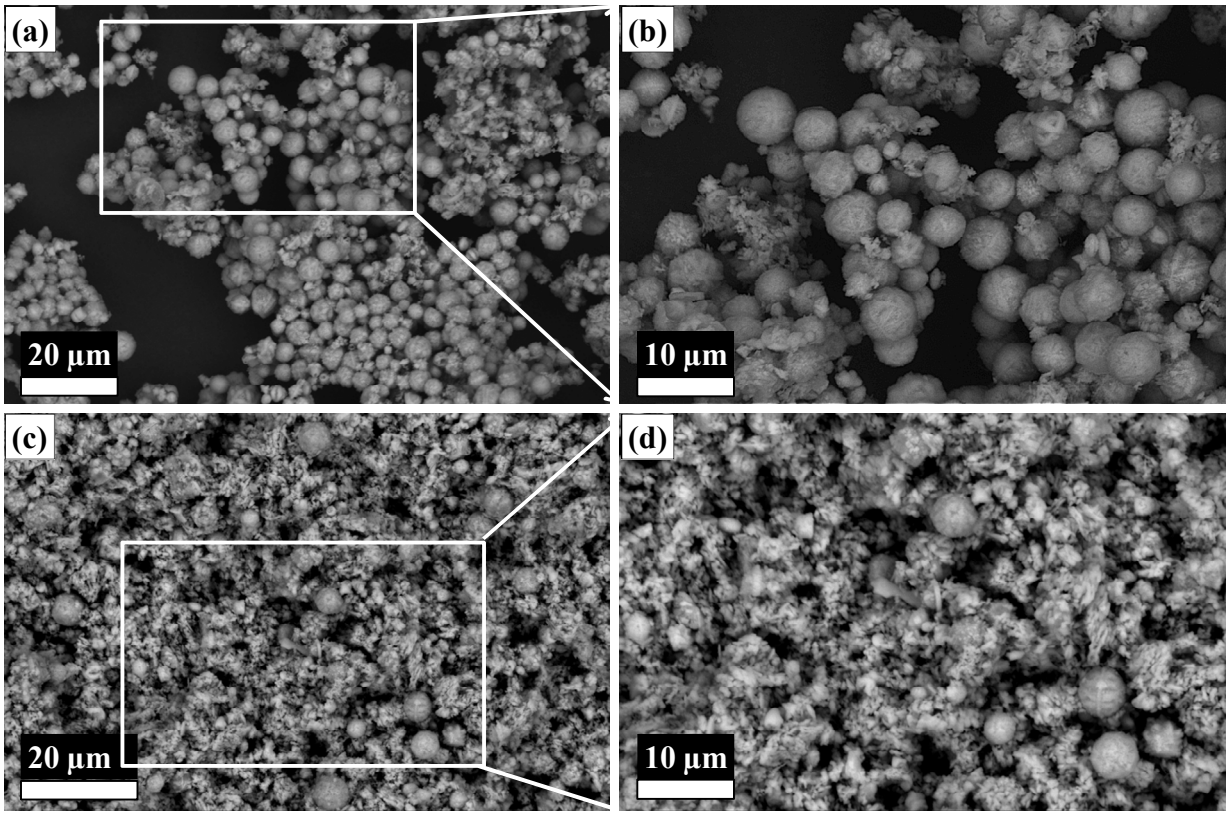

Fig. 4

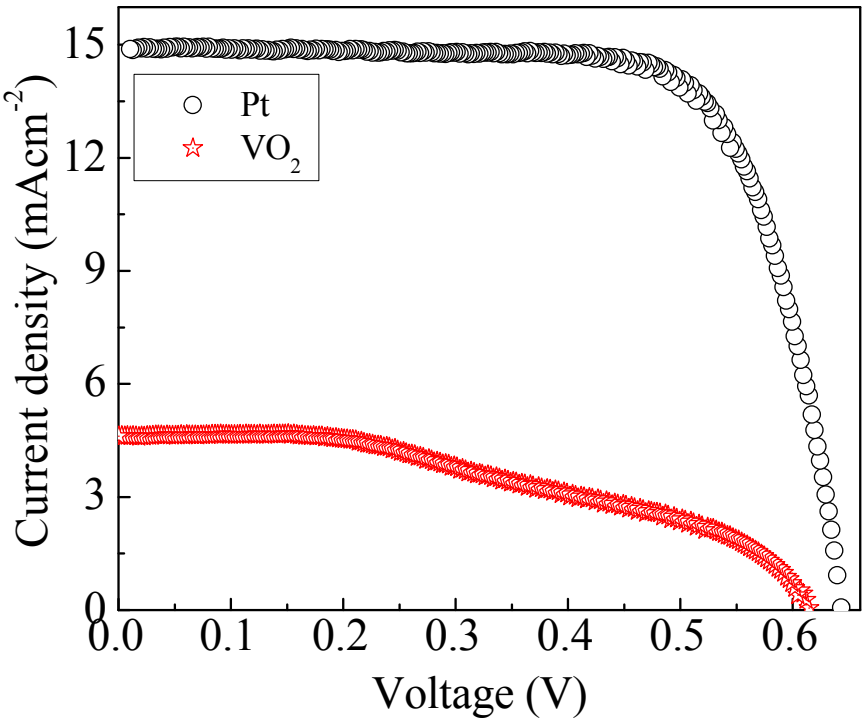
Current density (mAcm-2)
Voltage (V)
Pt
VO2
0
3
6
9
12
15
0.0
0.1
0.2
0.3
0.4
0.5
0.6

Fig. 5

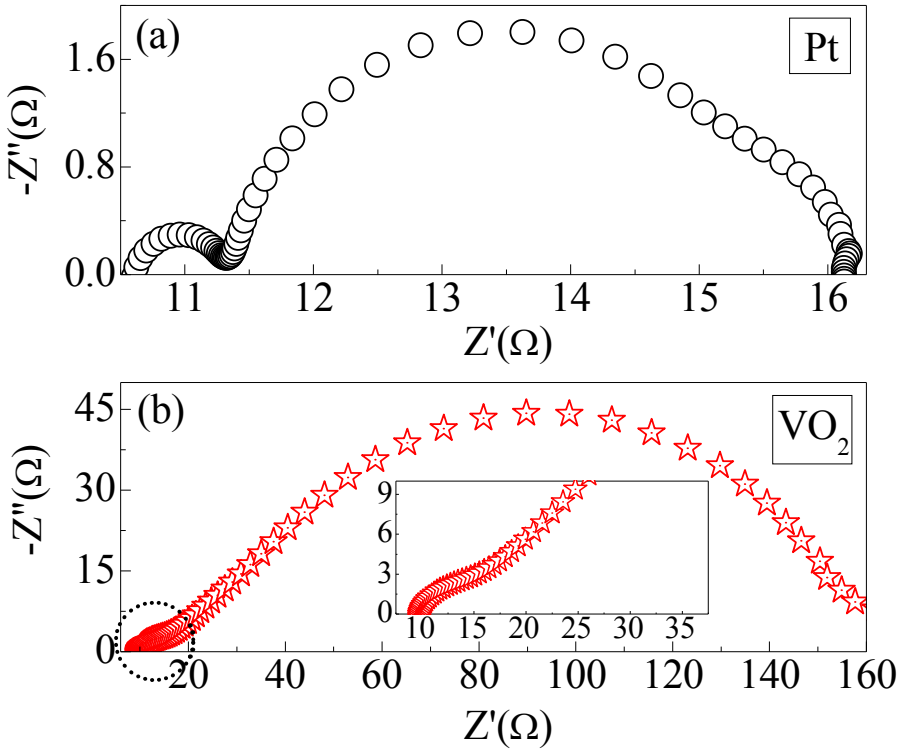
(a)
Pt
1.6
0.8
0.0
-Z''(Ω)
11
12
13
14
15
16
Z'(Ω)
(b)
VO2
45
30
15
0
-Z''(Ω)
9
6
3
0
10
15
20
25
30
35
20
40
60
80
100
120
140
160
Z'(Ω)

Fig. 6

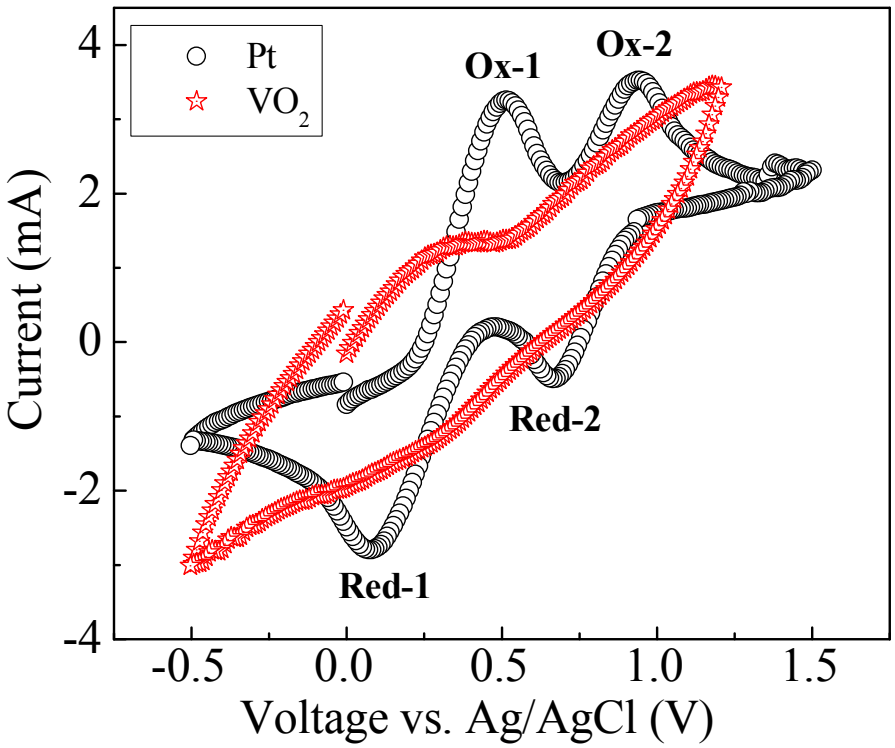
Pt
VO2
Ox-1
Ox-2
Red-1
Red-2
Current (mA)
Voltage vs. Ag/AgCl (V)
4
2
0
-2
-4
-0.5
0.0
0.5
1.0
1.5